NTS- 927

Open-File Report 80-1263

UNITED STATES
DEPARTMENT OF THE INTERIOR
GEOLOGICAL SURVEY

Analysis of the Magnetic Susceptibility Well Log in Drill Hole UE25a-5, Yucca Mountain, Nevada Test Site

by

J. T. Hagstrum, J. J. Daniels, and J. H. Scott

Open File Report 80-1263

1980

Prepared by the U.S. Geological Survey
for
Nevada Operations Office
U.S. Department of Energy
(Memorandum of Understanding DE-AI08-78ET44802)

TABLE OF CONTENTS

Abstract

Magnetic susceptibility measurements have been shown to be dependent upon the magnetite content of rocks with variations in rock susceptibility arising from changes in the shape, size, composition, and quantity of the contained magnetite grains. The present study was undertaken to determine the factor(s) responsible for the variation in magnetic susceptibility measurements from borehole UE25a-5 on the Nevada Test Site (NTS). The well logs and sample analyses presented in this paper form part of a larger geophysical well-logging project studying the physical properties of welded tuffs at NTS.

The ash-flow sheets at NTS appear to be the products of single compositionally zoned magmas that tend, within a cooling unit, to erupt hotter, more mafic, and more crystal-rich with time. These factors, however, have little effect on the degree to which the tuffs become welded. Furthermore, zones of crystallization and alteration are superimposed upon the welded units.

X-ray data show poor correspondence between the relative abundance of magnetite in a sample and the borehole magnetic susceptibility measurement associated with it. Curie balance experiments demonstrate no change in the magnetic mineralogy that could account for the susceptibility variation. Thin-section observations corroborate the X-ray data, but indicate a proportional relationship between the borehole susceptibility measurements and the grain-size distribution of magnetite. The association of magnetic susceptibility anomalies with the crystal-rich zones of the welded tuffs will aid in the identification and correlation of the eruptive sequences at NTS.

Introduction

There have been several studies made to demonstrate that the magnetic susceptibility of a rock containing a few percent ferrimagnetic minerals is linearly dependent on the magnetite content of the rock (Mooney and Bleifuss, 1953; Rao, 1956; Zablocki, 1974). For most rocks, the data are usually scattered enough to preclude the establishment of a precise numeric relationship; however, susceptibility-magnetite correlations have been shown to be a relatively inexpensive and reliable technique in iron-ore assessment (Shandley and Bacon, 1966; Zablocki, 1974). The scatter is attributed to the variation in the magnetic susceptibility of magnetite grains due to their shape, size, and orientation (Rao, 1956; Nagata, 1961; Kahn, 1962).

Magnetic susceptibility measurements were made in drill holes UE25a-4, -5, -6, and -7 at the Nevada Test Site (NTS) as part of a larger geophysical well-logging project investigating the physical properties of welded tuffs to assist in evaluating the potential of the tuffs as storage sites for radioactive waste. In-situ physical properties information is an important factor in surface geophysical data interpretation, aids in determining subsurface structures and stratigraphic correlations, and provides evidence bearing on the origin and emplacement of the rock units studied.

Because the relative magnetite content of the welded tuffs in drill hole UE25a-5 at NTS showed little relation to the borehole magnetic susceptibility measurements, this study was conducted to determine which aspect (or combination of aspects) of the magnetite grains is responsible for the variation found in the magnetic susceptibility logs.

Geologic Considerations

Erupted from the Timber Mountain-Oasis Valley caldera complex in late Tertiary time (16-9 m.y.), as much as 3000 m of rhyolitic tuffs at NTS mantle a portion of the basin and range province. In recent years, the tuff units and their associated calderas have been the subject of mapping and detailed study by the U.S. Geological Survey (Byers, et al, 1976; Christiansen, et al, 1977).

The ash-flow and bedded tuff sequences at NTS have been classified as stratigraphic units primarily on the basis of genetic relationships and cooling histories. The cooling histories of the tuff units determine the degree to which they become welded and are due largely to the temperature of emplacement and the thickness of the cooling units (Smith, 1960). The degree to which the ash flows become welded, for the most part, is independent of the temperature and composition of the erupted magma, although both progressively change through time, within a cooling unit, becoming higher and more mafic, respectively (Hildreth, 1979).

Zones of crystallization and alteration are superimposed on the variously welded portions of the vitric tuffs, although their presence may be dependent upon the degree of welding. Devitrification of the pyroclastic flows has occurred throughout almost all the densely welded portions of the tuffs. Associated with the thickest (>75m) densely welded zones are inner cores characterized by lithophysal cavities. These cavities are nearly spherical, mainly unconnected voids that are commonly lined with secondary minerals, primarily alkali feldspar and cristobalite. Vapor-phase minerals that crystallize from the hot volatiles released by the cooling tuff units are found mostly as linings of lenticular vugs. Alteration of the tuffs by ground water has resulted in zones of zeolitization, silicification, and calcitization.

The systematic chemical and mineralogical zonations of ash-flow sheets is best displayed by the Topopah Spring Member of the Paintbrush Tuff in the Yucca Mountain Section. The other units are represented in this section by more distal portions of the ash-flow sheets in which the densely welded crystalline cores thin, and towards the edges, disappear altogether. A compound cooling unit (partial cooling between flows), the Topopah Spring grades from a crystal-poor (1 percent phenocrysts) rhyolite at its base upward into a crystal-rich (21 percent phenocrysts) quartz latite caprock (Lipman, et al, 1966). The degree of flattening of pumice lenses in the caprock shows it to be the most densely welded part. Petrologic and chemical data indicate that the Topopah Spring was erupted from a single compositionally zoned magma chamber in inverted order to that observed in the ash-flow sheet. Although the variation in phenocryst content suggests magmatic differentiation by crystal settling, this mechanism is not supported by phenocryst proportions and chemical as well as geologic considerations, and the phenocryst variation is believed to be the product of progressive crystallization in place (Lipman, et al, 1966).

Borehole Magnetic Susceptibility Measurements

Borehole susceptibility instruments operate by measuring changes in the inductance of a coil produced by contrasts in the reluctance of the external magnetic path around it that are related to contrasts in formation susceptibility (Broding, et al, 1952). The sensing coil consists of a solenoid made of copper wire wound on a high-premeability ferrite core. The solenoid is connected as the unknown arm of a Maxwell inductance bridge that provides an unbalanced signal that is compared to a reference signal produced by a down-

hole oscillator. Variations in borehole diameter, centering of the coil in the borehole, and borehole temperature all affect the susceptibility measurements and must be accounted for in the design and calibration of the probe. The axis of the coil is oriented parallel to that of the borehole and the length of the coil determines the depth of penetration into the formation and the vertical resolution that may be expected in delineating thin beds of anomalous susceptibility. The coil length in the probe used to make the measurements of this study was 30.48 cm. The depth of penetration is approximately equal to this value, and high susceptibility beds thinner than the coil length will produce a truncated double anomaly on the record as the field intensive ends of the probe pass by.

Discussion of Magnetic Susceptibility Results in Welded Tuffs

The magnetic susceptibility logs made in drill holes UE25a-4, -5, -6, and -7 are shown in figure 1; the stratigraphic units of the region are assigned to depth intervals within the holes as determined by Spengler and Rosenbaum (1980). The anomaly pattern is similar in all four holes and the distinct features of the patterns that correspond to one another are consistent with single stratigraphic horizons. Anomalies 5-I and 6-V appear smaller than corresponding anomalies in other holes due to the thin-bed effect (bed thickness < coil length) discussed in the last section. Because the core samples are so much smaller than, and possibly misrepresentative of, the volume of rock sensed by the probe, laboratory susceptibility measurements were made on 13 samples from holes UE25a-4 and -5. The laboratory values correspond well with those made by the borehole instrument (figure 2).

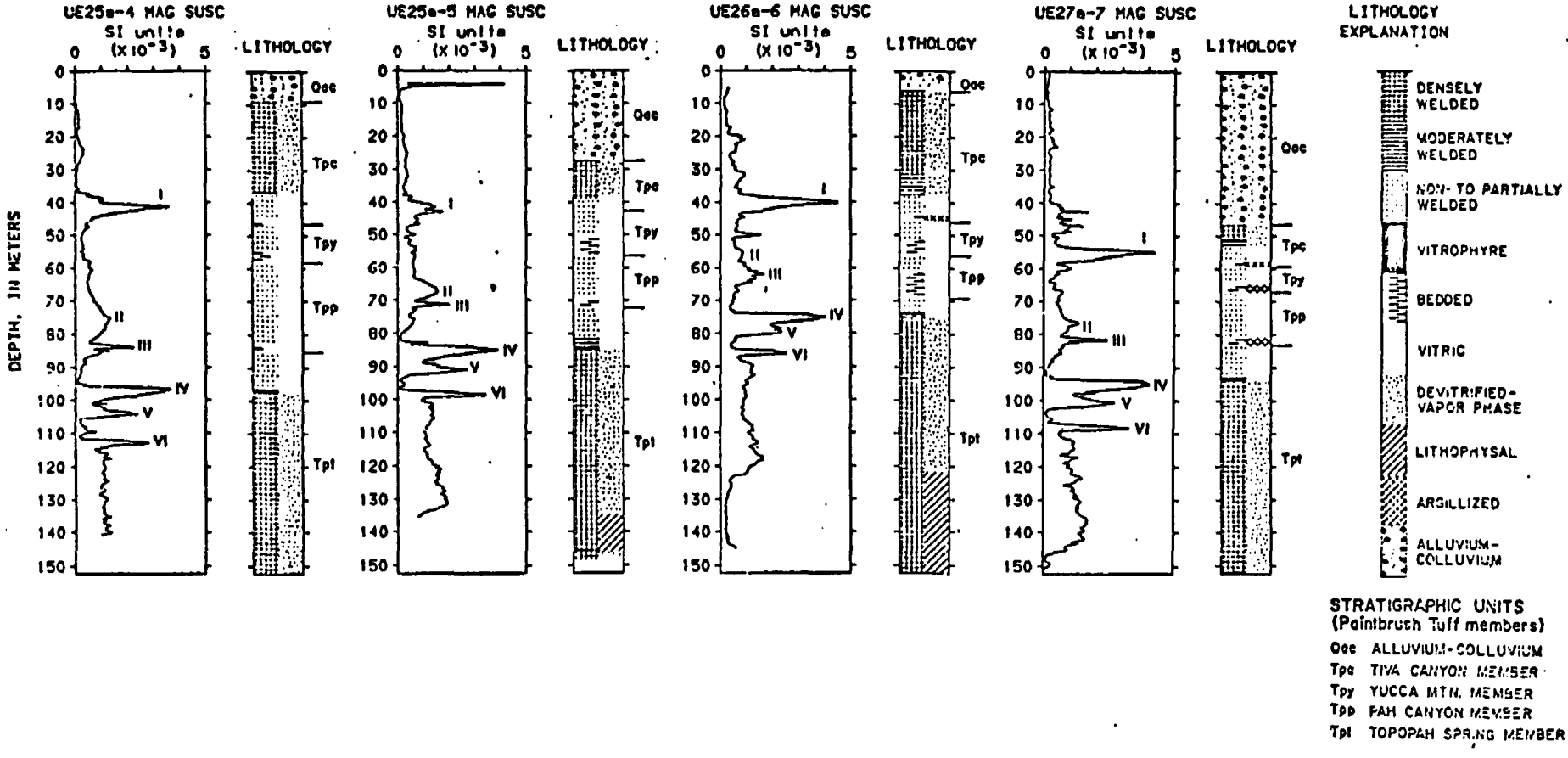

Figure 1.--Magnetic susceptibility well logs from drill holes UE25a-4, -5, -6, and -7, Nevada Test Site, with lithology, crystallized and altered zones (left and right sides of lithology columns, respectively), and stratigraphic units assigned to depth intervals as determined in Spengler and Rosembaum (1980).

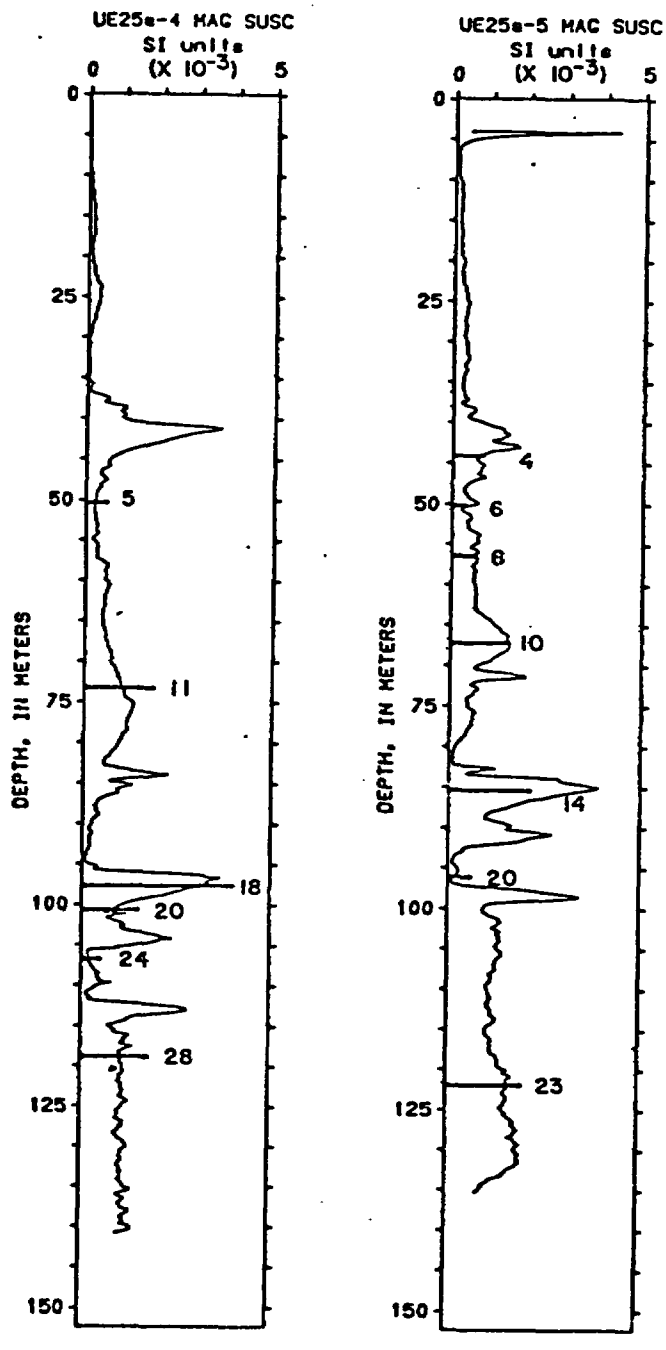

Figure 2.—Laboratory susceptibility measurements on 13 samples from holes UE25a-4 and -5, Nevada Test Site, superimposed on the borehole susceptibility logs.

The X-ray diffraction work on core samples from drill hole UE25a-5 revealed a variation in magnetite and hematite content that are shown in figure 3 (Paul Blackmon, written commun., 1980). Inspection of these data indicate that the large anomalies labeled in figure 1, hole 5, occur only where magnetite is found to be present and that the lowest values correspond primarily to samples in which magnetite is present in relatively low amounts or is absent. These low susceptibility values in the presence of substantial quantities of the ubiquitous hematite grains illustrate the dependence of magnetic susceptibility of a rock on its magnetite content rather than on its hematite content. A further comparison of figure 1 (drill hole UE25a-5) and figure 3 shows that the relative amplitudes of the various anomalies appear to be independent of the quantity of magnetite observed in the core samples (figure 4). The magnetic susceptibility anomalies, therefore, seem to be caused by an aspect of the magnetite grains that overshadows the effect of the relative abundance of the grains.

Curie-balance experiments were performed on a number of core samples (table 1) from drill hole UE25a-5 to detect any change in the magnetic mineralogy with depth. All but one sample were characteristic of magnetite giving a Curie temperature of approximately 560°C. Representative examples are given in figure 5). The experiments were conducted in air, which resulted in oxidation of the magnetite particles to hematite as evidenced by the reduced saturation magnetization (Js) values on the decreasing temperature path. Sample 17 exhibited a Neel temperature of approximately 630°C indicating only the presence of hematite, because any magnetite in the sample would dominate the response (figure 5). This result corraborates the X-ray diffraction work that showed no magnetite present in sample 17. The Curie-balance and X-ray

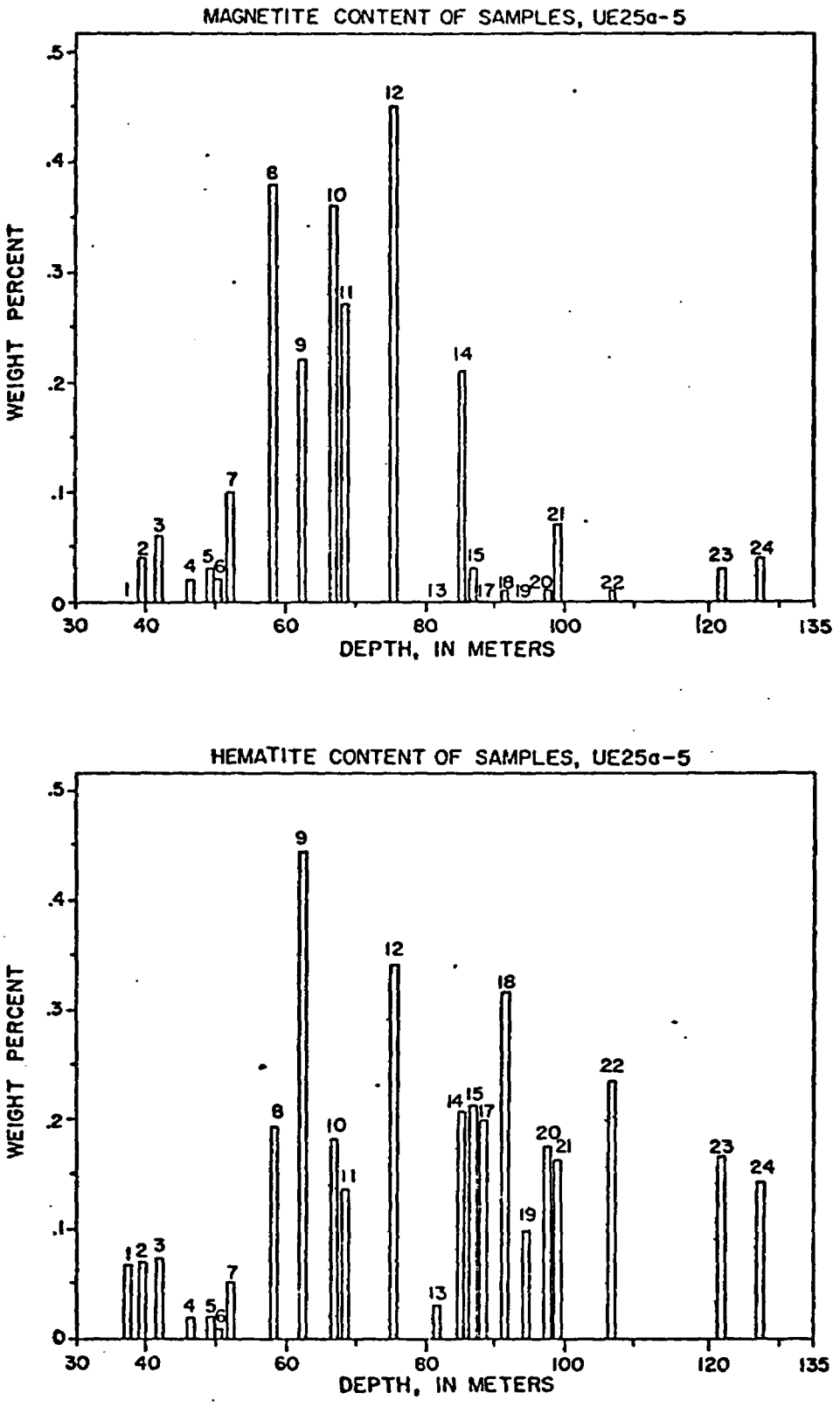

Figure 3.—Magnetite and hematite content in weight percent of samples from drill hole UE25a-5, Nevada Test Site, (Paul Blackmon, written commun., 1980).

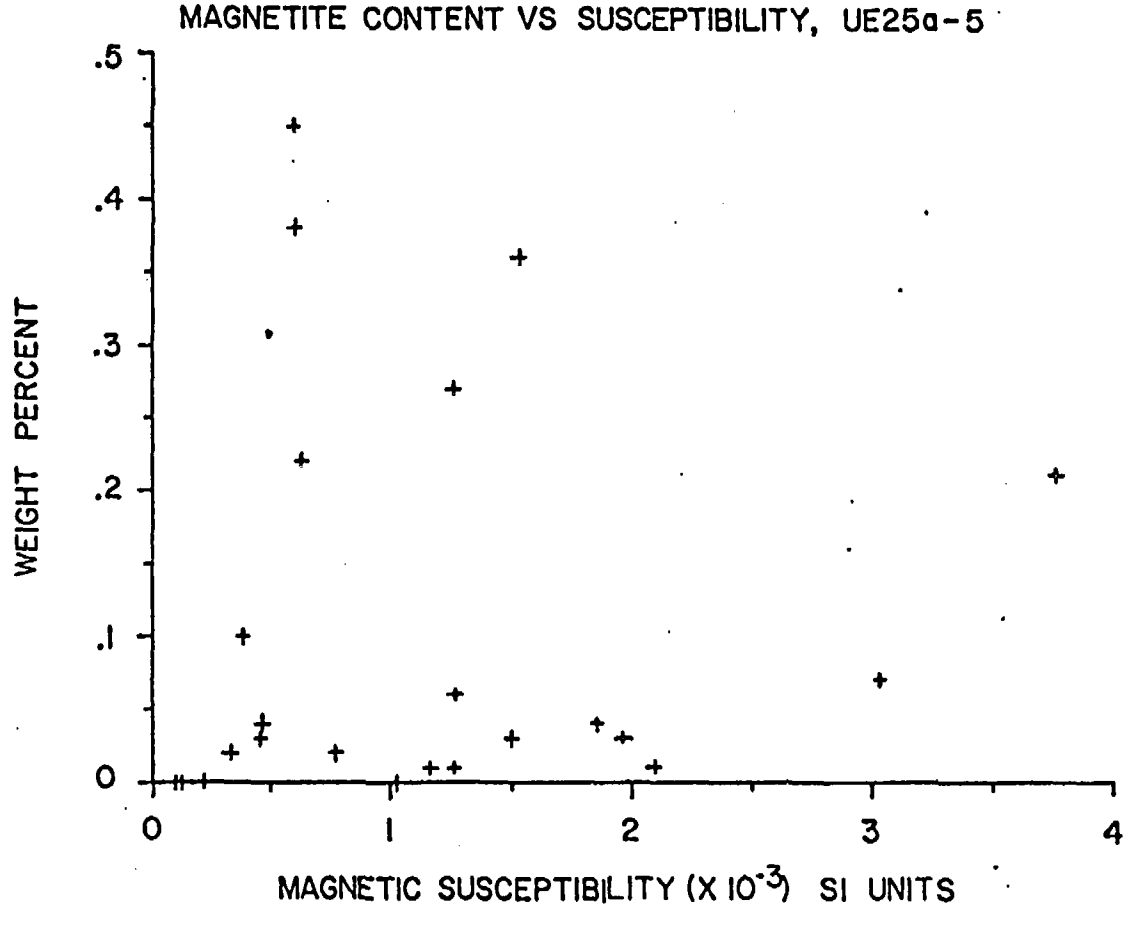

Figure 4.--Weight percent magnetite of samples from drill hole UE25a-5, Nevada Test Site, plotted against borehole magnetic susceptibility measurements from corresponding depths.

Table 1. Sample Analyses from Drill Hole UE25a-5, Nevada Test Site

Sample No.	Depth m	Mag. Susc. SI Units ($x10^{-3}$)	Thin section	Curie balance	Magnetite content, weight percent	Average magnetite grain diameter, microns	Members of Paintbrush Tuff
1	37.5	.2298	X		0	-	Tiva
2	39.6	.4898	X	X	.04	153.9	Canyon
3	42.1	1.3459	X		.06	115.3	Member
4	46.6	.8174		X	.02		
5	49.4	.4789			.03		Yucca
6	50.4	.3479		X	.02		Mountain
7	52.2	.4029			.10		Member
8	58.5	.6291		X	.38	78.0	
9	62.5	.6603			.22		Pah
10	67.1	1.6201	X	X	.36	66.7	Canyon
11	68.6	1.3390			.27		Member
12	75.5	.6258		X	.05		
13	81.7	.1047	X		0	-	
14	85.3	3.9955	X	X	.21	161.5	Topopah
15	86.9	2.0868			.03		Spring
17	88.3	1.0835	X	X	0	-	Member
18	91.4	2.2264	X		.01	88.9	
19	94.5	.1315	X		0	-	
20	97.5	1.2326			.01		
21	98.9	3.2194	X		.07	170.1	
22	106.6	1.3387			.01		
23	122.0	1.6012			.03		
24	127.6	1.9813	X	X	.04	122.0	

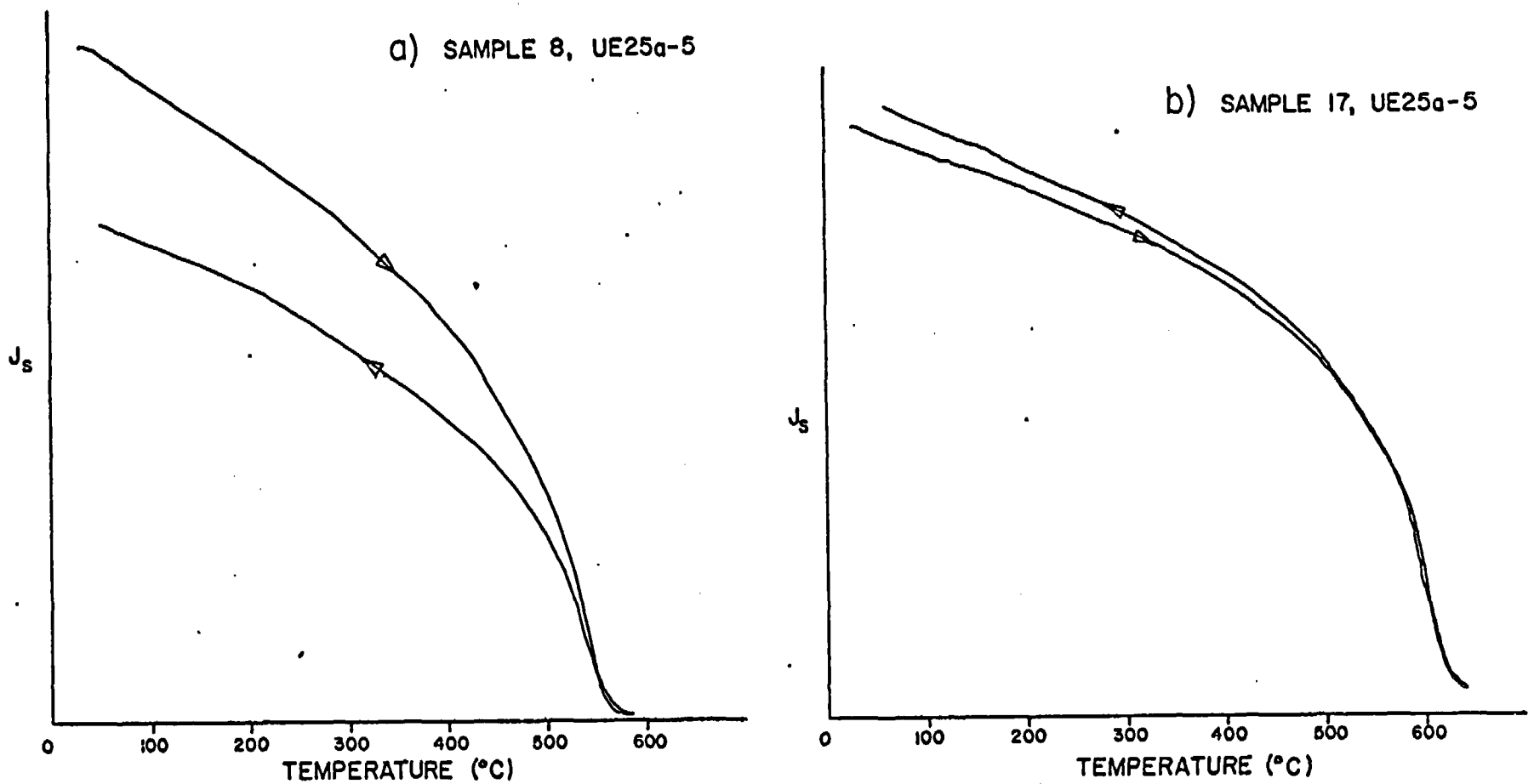

Figure 5.--Curie-balance experiments on heavy separate minerals from samples 8 and 17 from drill hole UE25a-5, Nevada Test Site. Sample 8 exhibits representative behavior for those samples that contained magnetite, and sample 17 shows no magnetite present, demonstrating behavior typical of hematite.

diffraction results indicate that only magnetite and no other magnetic mineral is responsible for the susceptibility anomalies seen in figure 1.

Thin sections of 12 core samples from UE25a-5 (table 1) were cut and polished to observe the geometric and textural nature of the magnetic grains contained within the welded tuffs. Appendix A gives histograms of numbers versus area for the magnetite and hematite grains seen in each of the thin-sectioned core samples. Diameters of equidimensional grains were measured directly, whereas non-equidimensional grains were measured along their major and minor axes defining a rectangular area (Appendix A) that was converted to a diameter representing an equivalent circular area. Figure 6 shows the average magnetite grain diameters for thin-sectioned samples plotted against depth. Grains were usually close to equidimensional, and rarely passed beyond a 1.5:1 major to minor axis ratio. Grains with major axes less than 30 microns were not recorded. No preferred orientation of the grains was observed and none was expected in light of the turbulent and rapid mode of emplacement for this rock type. All magnetite grains observed in thin section from drill hole UE25a-5 were oxidized to some degree to hematite with minor amounts of exsolved ilmenite and spinel present. The hematite occurred primarily along rims, cracks, and crystallographic axes ({111}) of the magnetite grains. Some magnetite grains had been almost totally replaced by hematite, whereas others appeared relatively fresh. In general, the more oxidized magnetite grains were found in the nonwelded portions of the tuffs, and the least oxidized magnetite grains tended to be associated with the more densely welded portions of the tuffs.

Figure 7 illustrates the relationship between the grain diameter and magnetic susceptibility measurements in drill hole UE25a-5. A least-squares

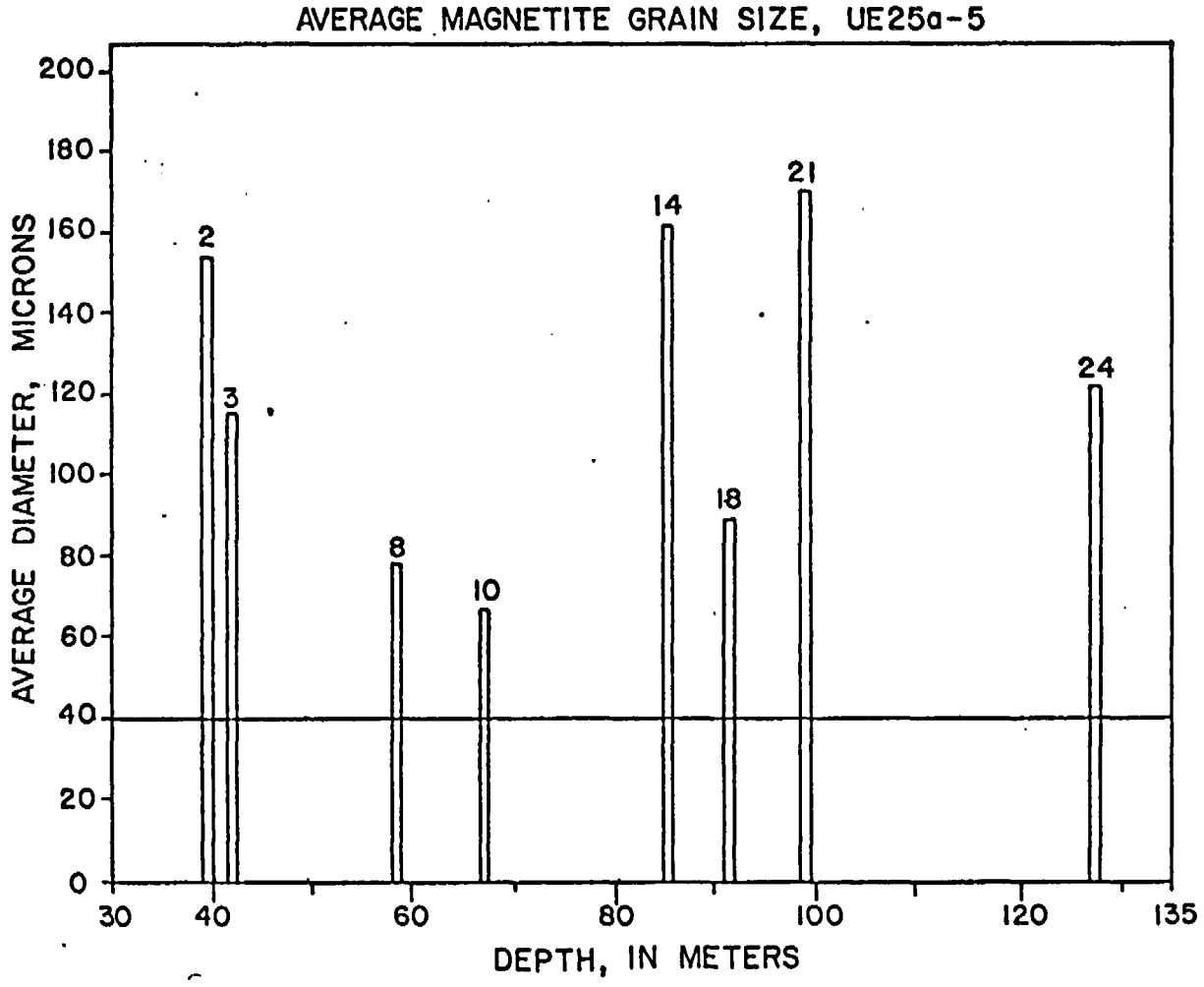

Figure 6.--Average magnetite grain diameters for samples, determined from thin-section observations, from drill hole UE25a-5, Nevada Test Site. The line at 40 microns represents an experimental cutoff below which the magnetic susceptibility of magnetite grains was observed to sharply decrease (figure 7).

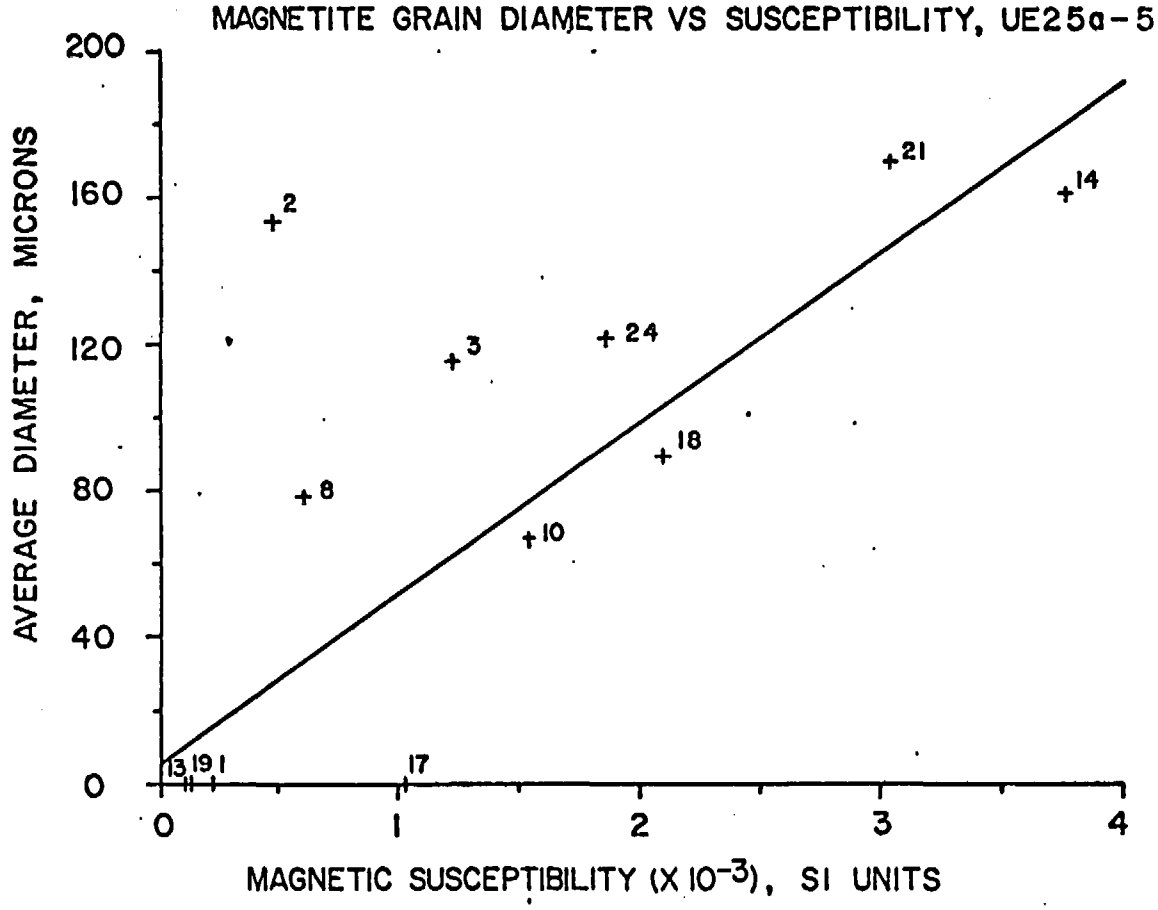

Figure 7.--Average magnetite grain diameter of samples from drill hole UE25a-5, Nevada Test Site, plotted against borehole magnetic susceptibility measurements from corresponding depths. The line represents a least-squares fit of all but one point representing sample 2 (see text).

fit of the points yields the equation: susceptibility = 62.5 x grain diameter. Sample 2 was not included in the construction of the line because the magnetic susceptibility measurement associated with this depth is inaccurate due to a thin-bed effect for this anomaly (figure 1, 5-I). A correction for sample 2 could be obtained from figure 7 by increasing its susceptibility value along a line of fixed grain diameter until the least-squares line is intersected. This susceptibility value is similar to those recorded for the other holes at this horizon where the high-susceptibility bed is thick enough (>30.48 cm) to permit an accurate borehole measurement (figure 1, 4-I, 6-I, 7-I). Figure 8 presents an experimental relationship between magnetic susceptibility and synthetic mixtures of sand and magnetite particles (5 percent) of varying size determined by Shandley and Bacon (1966). These data demonstrate a sharp decrease in magnetic susceptibility for grains with diameters less than about 40 microns. The line representing 40 microns has been drawn across figure 6, and does not separate the large diameter grain-small magnetite content-high susceptibility samples (2, 3, 14, 18, 21, 24) from the small diameter grain-large magnetite content-low susceptibility samples (8, 10) as expected. The arbitrary cutoff of a 30-micron diamter, below which grain sizes were not counted, tend to bias the grain-size count upward. The magnetite grain-size distribution histograms for samples 8 and 10 in Appendix A appear to be the upper ends of standard bell-shaped distributions that suggest a mean grain diameter for these samples far less than those presented in figure 6. Many grains smaller than 30 microns were observed in the thin sections from these two samples. Another factor that may have bearing on this discrepancy could be, in effect, the reduction of grain size due to exsolution and oxidation textures. Because magnetic susceptibility is dependent upon the

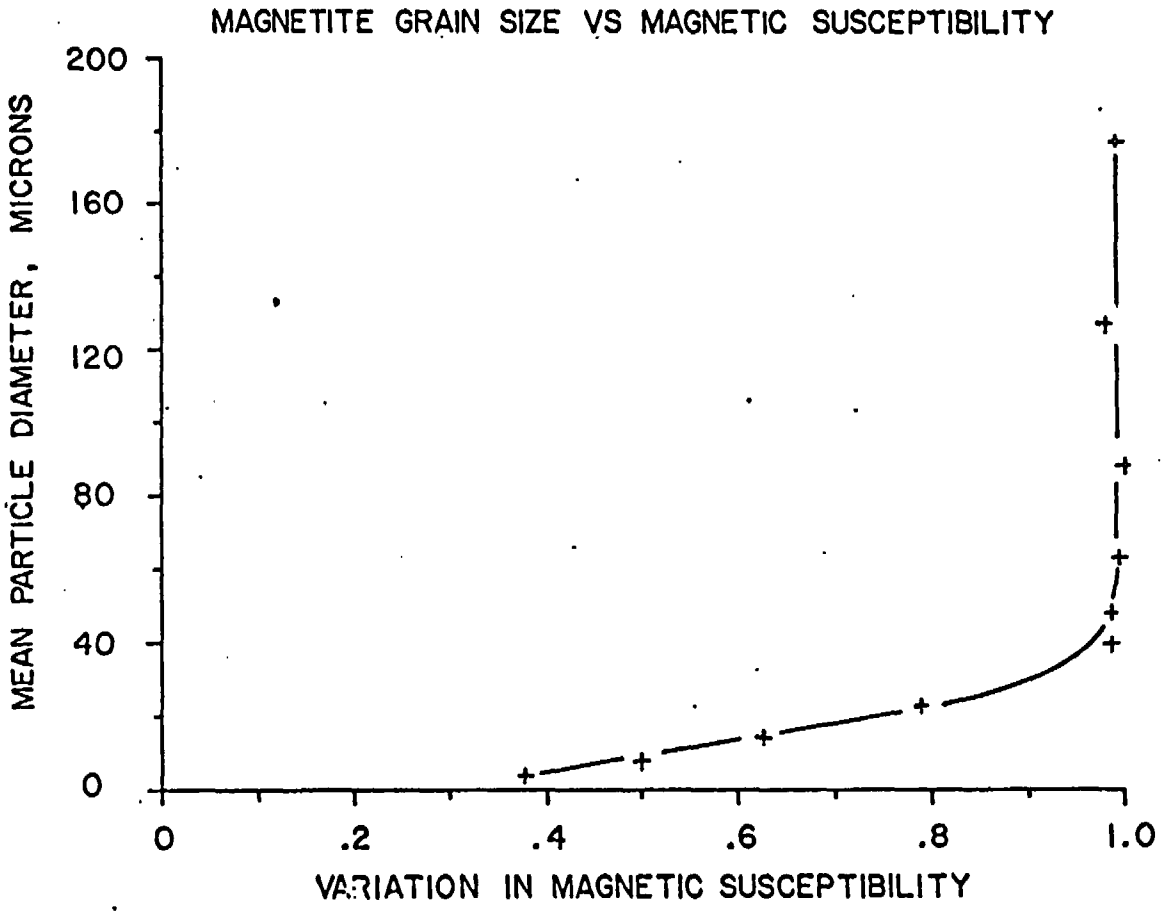

Figure 8.--Variation of magnetic susceptibility with change in grain size as determined by Shandley and Bacon (1966).

ease of domain wall movement within the magnetite grains, these textures would restrict their motion in the same manner as would a smaller grain diameter. This effect would also be most prevalent in the more oxidized magnetite grains associated with the less densely welded tuffs.

Conclusions

The magnetic susceptibility measurements in welded tuffs at NTS appear to be dominantly controlled by the average magnetite grain diameter in rock of varying grain size and by the amount of magnetite in rock of uniform grain size. The Curie-balance experiments and thin-section observations corroborate the X-ray diffraction data on samples from UE25a-5 by suggesting that other magnetic minerals, grain-shape orientations, and relative hematite abundance play insignificant roles in the borehole susceptibility measurements. The magnetite grain amounts and grain-size variations, in turn, are dependent upon the compositional zonations and the degree to which the magma has undergone crystallization prior to eruption. As a result, the systematic variation in texture and composition through time of the ash-flow sheets in a cooling unit, with the attendant change in magnetic susceptibility, enables the identification of eruptive sequences as well as detailed stratigraphic correlations between them based on magnetic susceptibility measurements. However, more work along the lines of this report is needed on data and core samples from other holes (UE25a-4, -6, -7) at NTS to further substantiate these preliminary results.

REFERENCES

Broding, R. A., Zimmerman, C. W., Somers, E. V., Wilhelm, E. S., and Stripling, A. A., 1952, Magnetic well logging: Geophysics, v. 17, no. 1, p. 1-26.

Byers, F. M., Jr., Carr, W. J., Orkild, P. P., Quinlivan, W. D., and Sargent, K. A., 1976, Volcanic suites and related caldrons of Timber Mountain-Oasis Valley caldera complex, southern Nevada: U.S. Geological Survey Professional Paper 919, 70 p.

Christiansen, R. L., Lipman, P. W., Carr, W. J., Byers, F. M., Jr., Orkild, P. P., and Sargent, K. A., 1977, Timber Mountain-Oasis Valley caldera complex of southern Nevada: Geological Society of America Bulletin, v. 88, p. 943-959.

Hildreth, W., 1979, The Bishop Tuff: Evidence for the origin of compositional zonation in silicic magma chambers: Geological Society of America Special Paper 180, p. 43-75.

Kahn, M. A., 1962, The anisotropy of magnetic susceptibility of some igneous and metamorphic rocks: Journal of Geophysical Research, v. 67, n. 7, p. 2873-2885.

Lipman, P. W., Christiansen, R. L., and O'Connor, J. T., 1966, A compositionally zoned ash-flow sheet in southern Nevada: U.S. Geological Survey Professional Paper 524-F, 47 p.

Mooney, H. M., and Bleifuss, R., 1953, Magnetic susceptibility measurements in Minnesota, Part II: Analysis of field results: Geophysics, v. 18, p. 383-393.

Nagata, T., 1961, Rock magnetism: Tokyo, Maruzen, 350 p.

Rao, V. B., 1956, Magnetic properties of magnetite: Geophysics, v. 21, n. 4, p. 1100-1110.

Shandley P. D., and Bacon, L. O., 1966, Analysis for magnetite using magnetic susceptibility: Geophysics, v. 31, n. 2, p. 398-409.

Smith, R. L., 1960, Ash flows: Geological Society of America Bulletin, v. 71, p. 795-842.

Spengler, R. W., and Rosenbaum, J. G., 1980, Preliminary interpretations of geologic results obtained from boreholes UE25a-4, -5, -6, and -7, Yucca Mountain, Nevada Test Site: U.S. Geological Survey Open-File Report 80-929, 33 p.

Zablocki, C. J., 1974, Magnetite assays from magnetic susceptibility measurements in taconite production blast holes, northern Minnesota: Geophysics, v. 39, n. 2, p. 174-189.

APPENDIX A

Magnetite and Hematite grain-size distributions in 12 samples from drill hole UE25a-5, Nevada Test Site

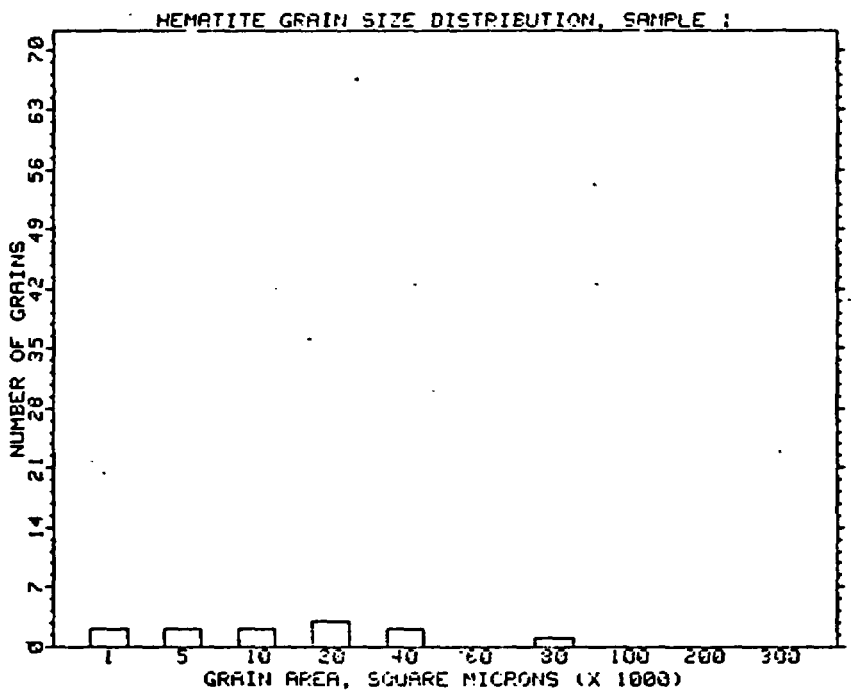

Figure A1.—Histogram of hematite grain-size distribution in sample 1 from drill hole UE25a-5, Nevada Test Site. Numbers below bars indicate maximum grain area in thousands of square microns.

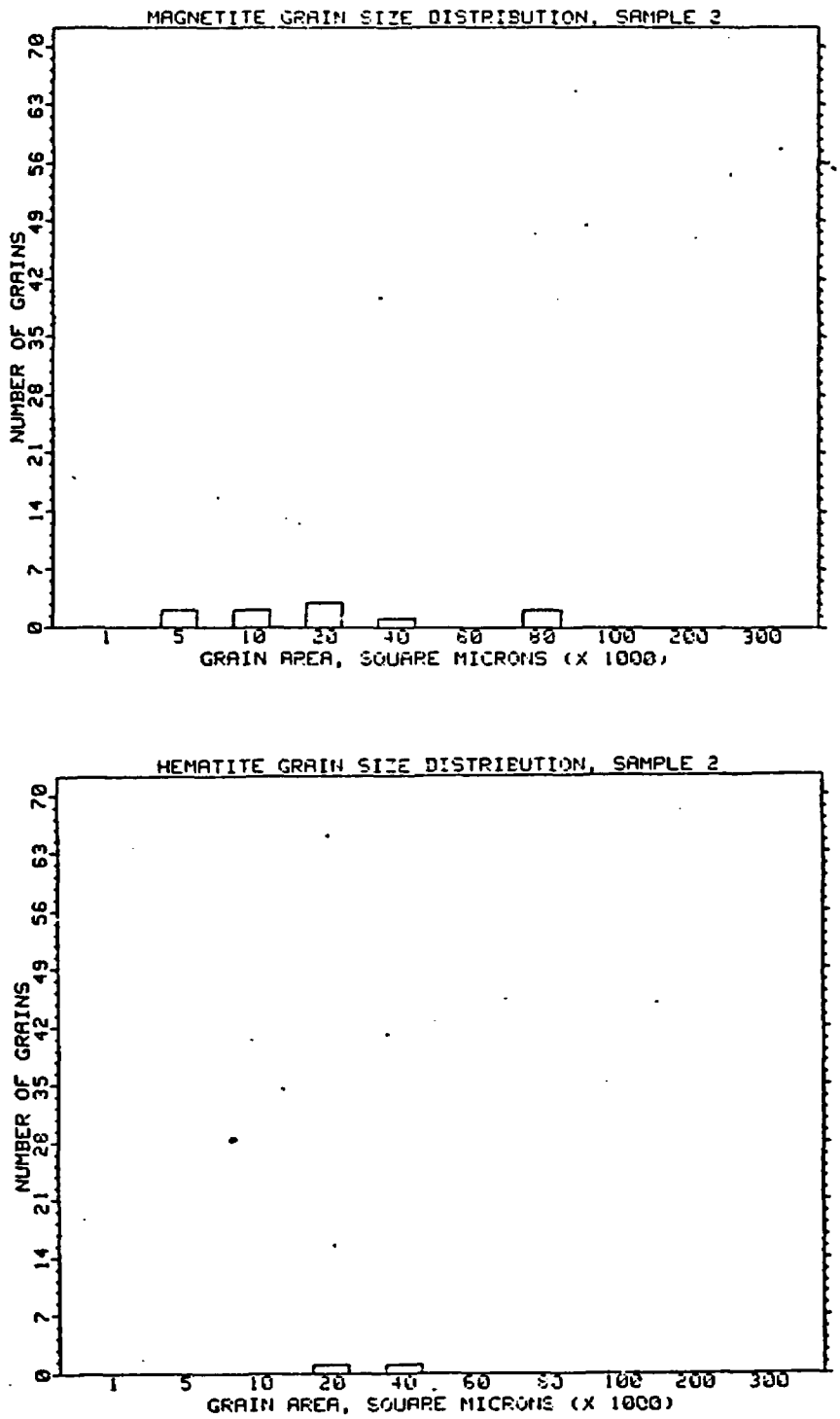

Figure A2.—Histogram of hematite and magnetite grain-size distributions in sample 2 from drill hole UE25a-5, Nevada Test Site. Numbers below bars indicate maximum grain area in thousands of square microns.

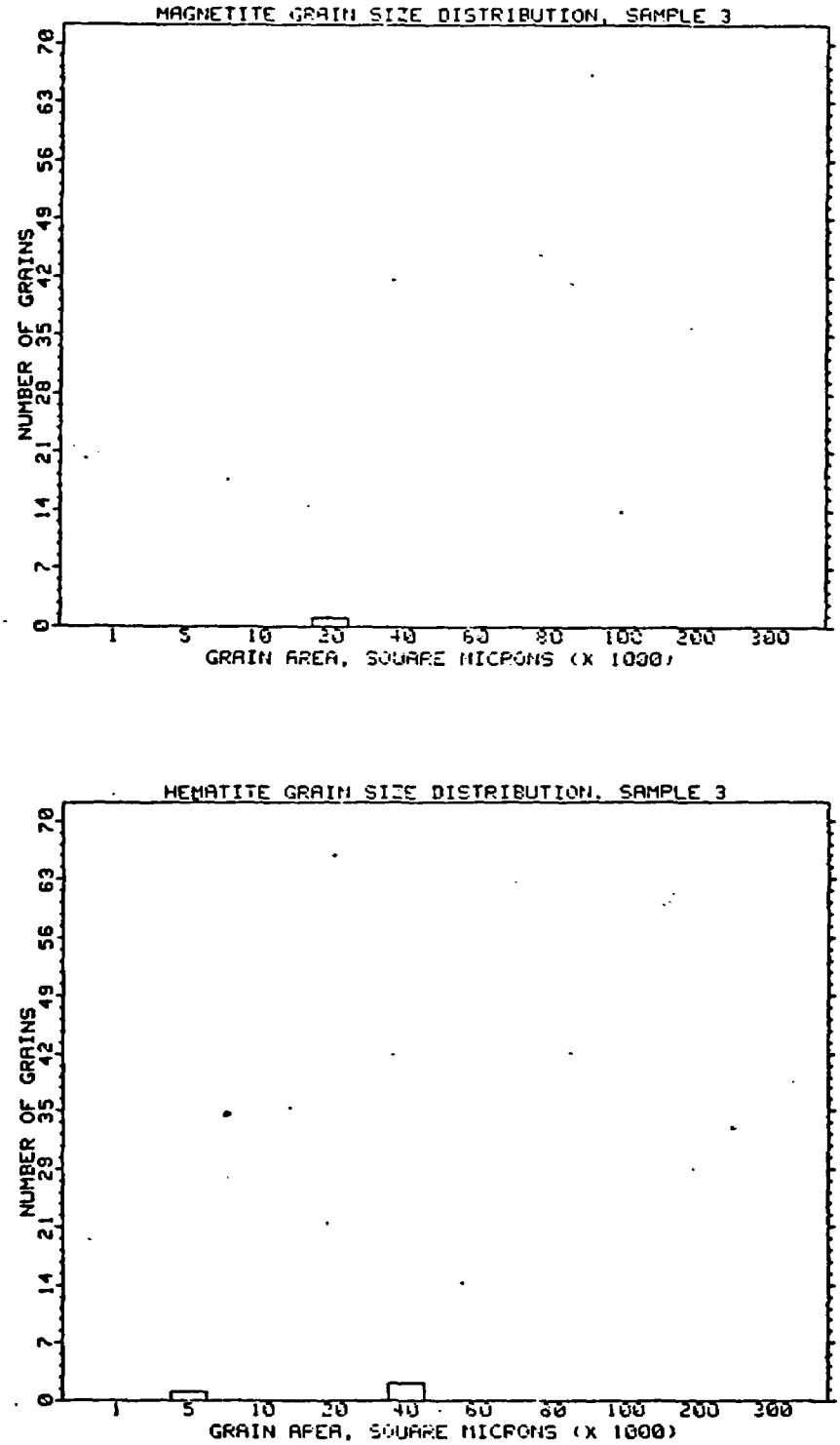

Figure A3.—Histogram of hematite and magnetite grain-size distributions in sample 3 from drill hole UE25a-5, Nevada Test Site. Numbers below bars indicate maximum grain area in thousands of square microns.

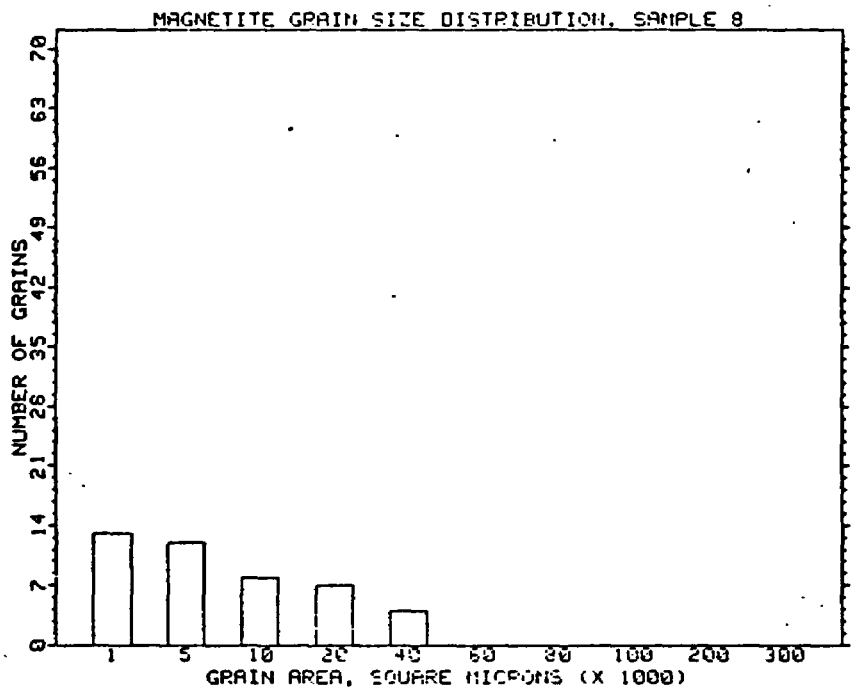

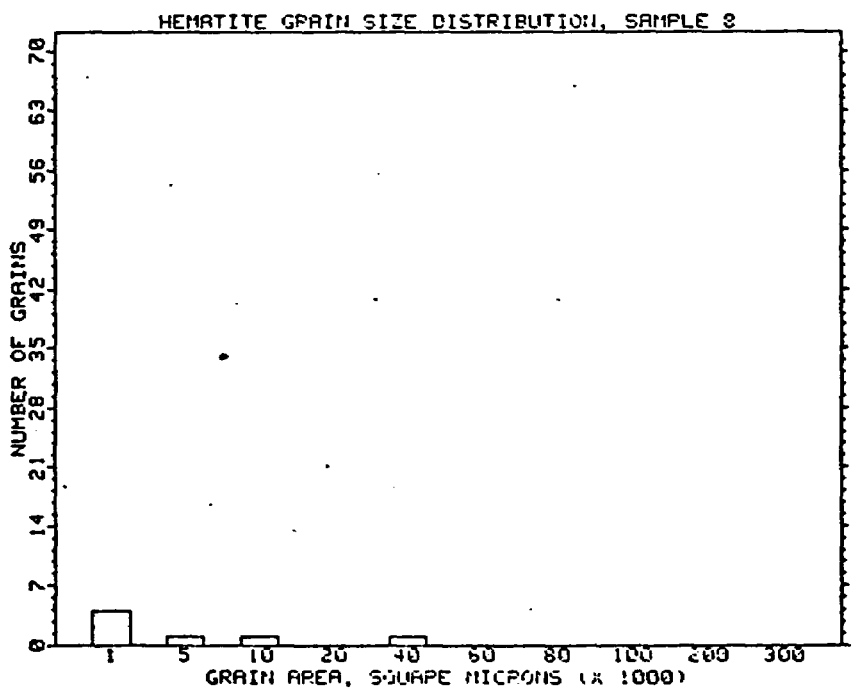

Figure A4.—Histogram of hematite and magnetite grain-size distributions in sample 8 from drill hole UE25a-5, Nevada Test Site. Numbers below bars indicate maximum grain area in thousands of square microns.

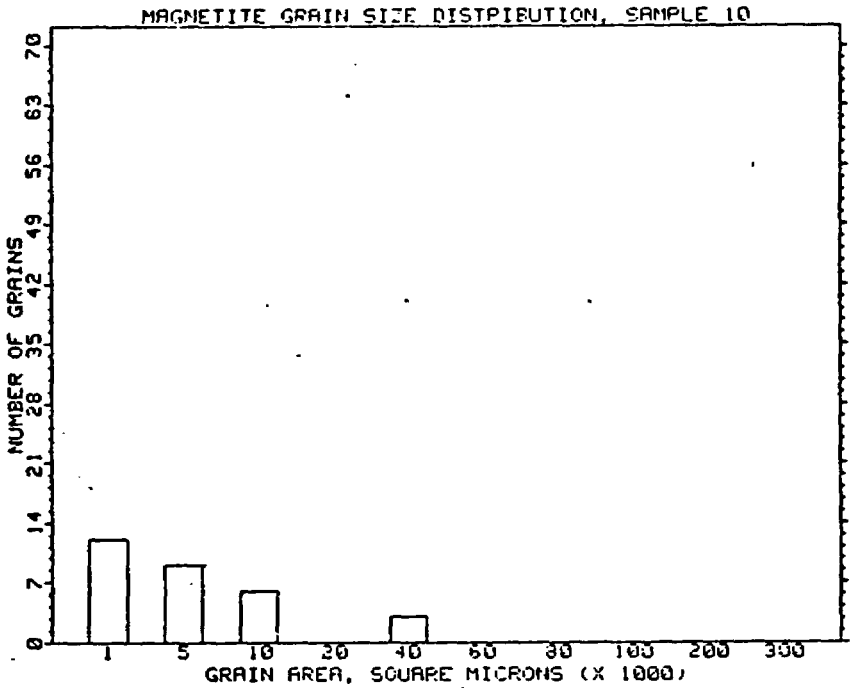

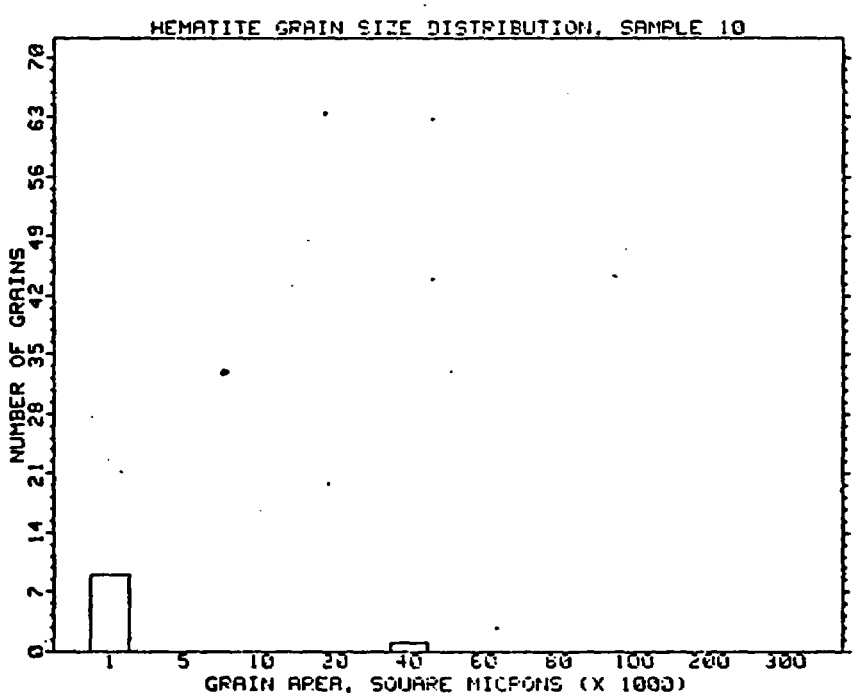

Figure A5.—Histogram of hematite and magnetite grain-size distributions in sample 10 from drill hole UE25a-5, Nevada Test Site. Numbers below bars indicate maximum grain area in thousands of square microns.

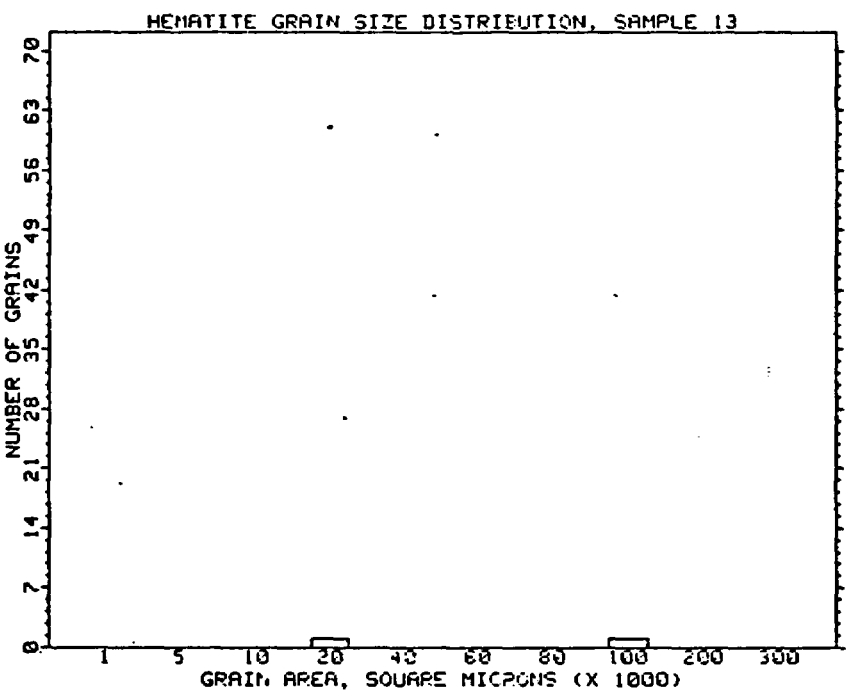

Figure A6.--Histogram of hematite grain-size distribution in sample 13 from drill hole UE25a-5, Nevada Test Site. Numbers below bars indicate maximum grain area in thousands of square microns.

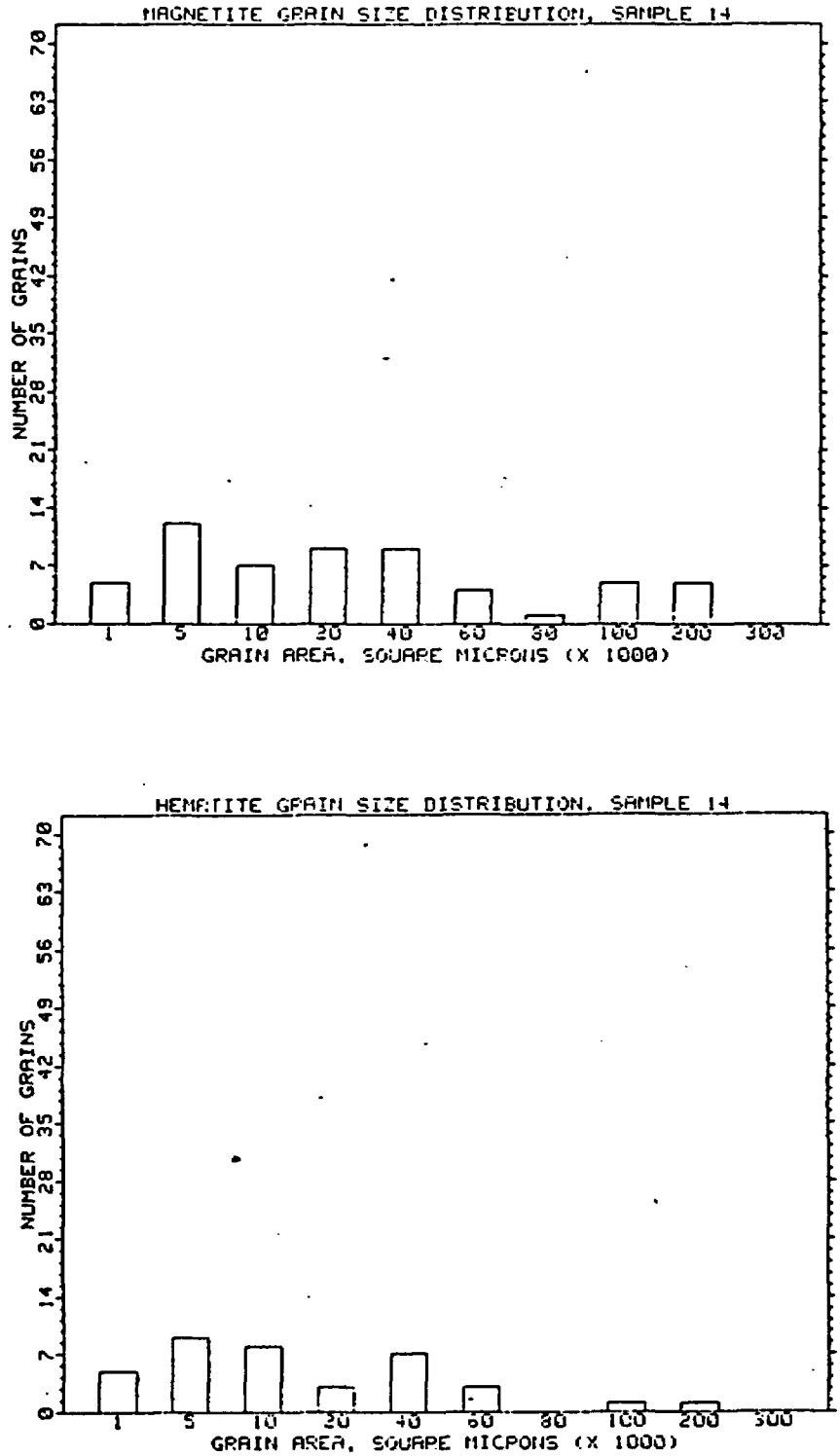

Figure A7.—Histogram of hematite and magnetite grain-size distributions in sample 14 from drill hole UE25a-5, Nevada Test Site. Numbers below bars indicate maximum grain area in thousands of square microns.

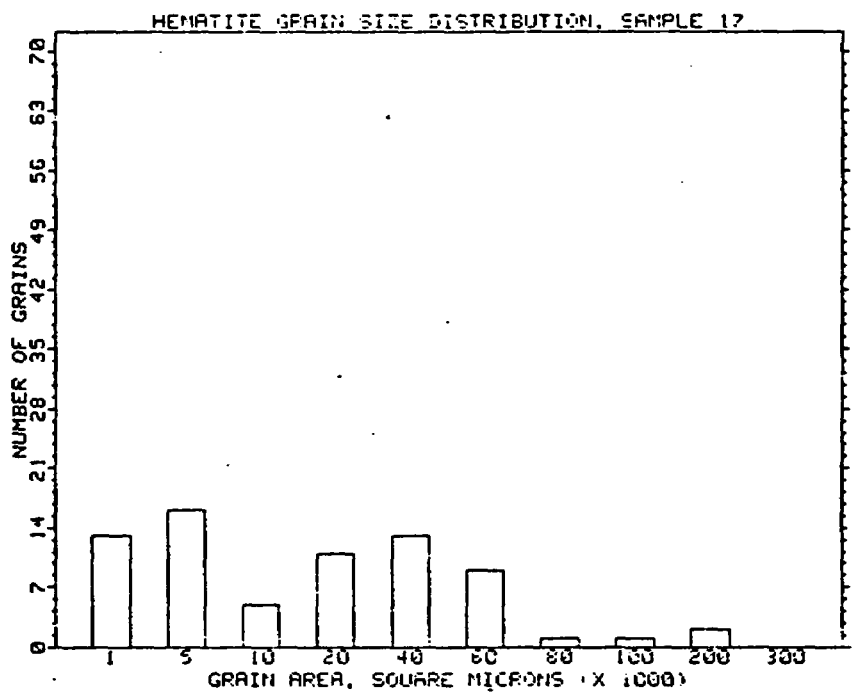

Figure A8.--Histogram of hematite grain-size distribution in sample 17 from drill hole UE25a-5, Nevada Test Site. Numbers below bars indicate maximum grain area in thousands of square microns.

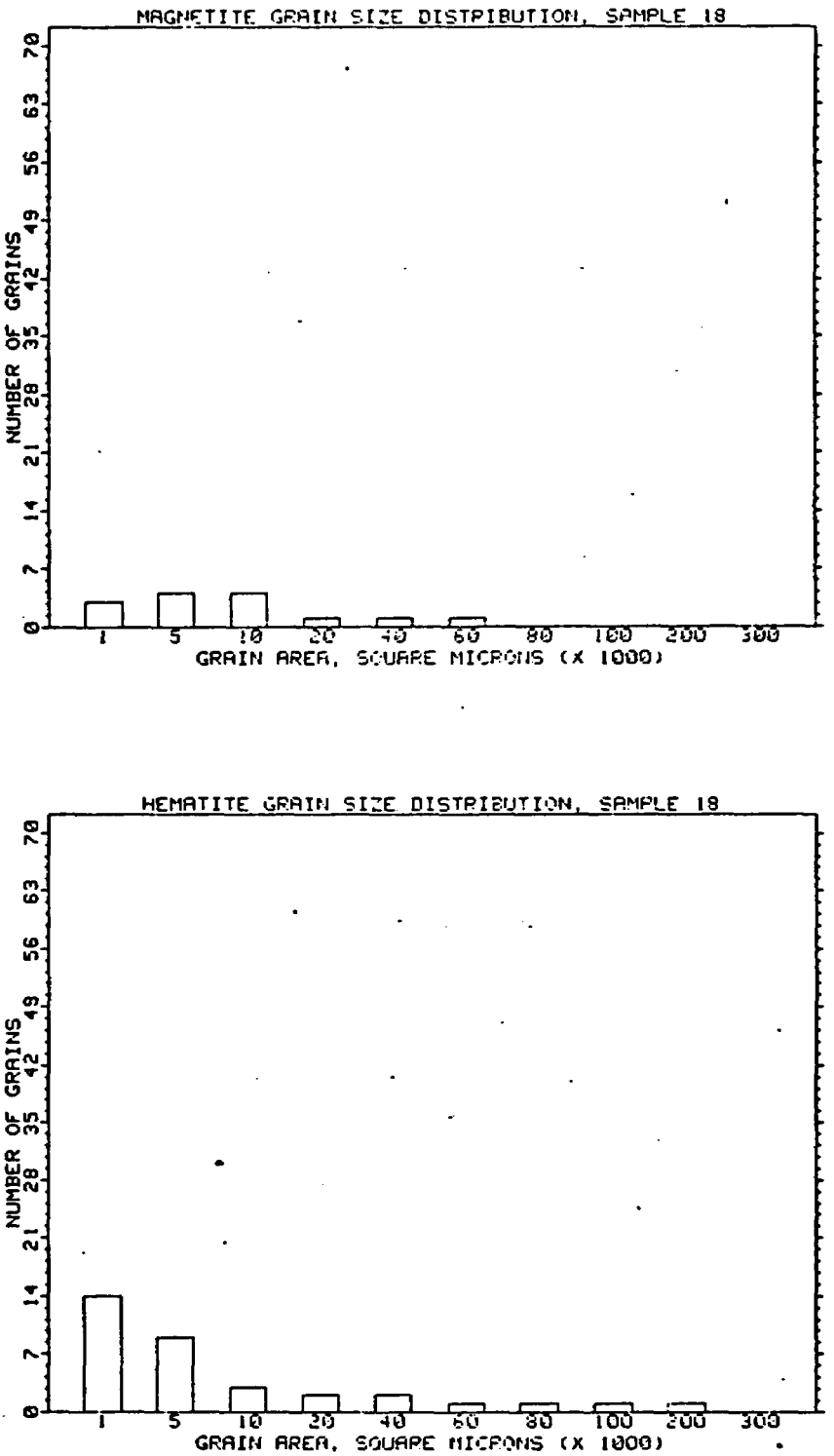

Figure A9.—Histogram of hematite and magnetite grain-size distributions in sample 18 from drill hole UE25a-5, Nevada Test Site. Numbers below bars indicate maximum grain area in thousands of square microns.

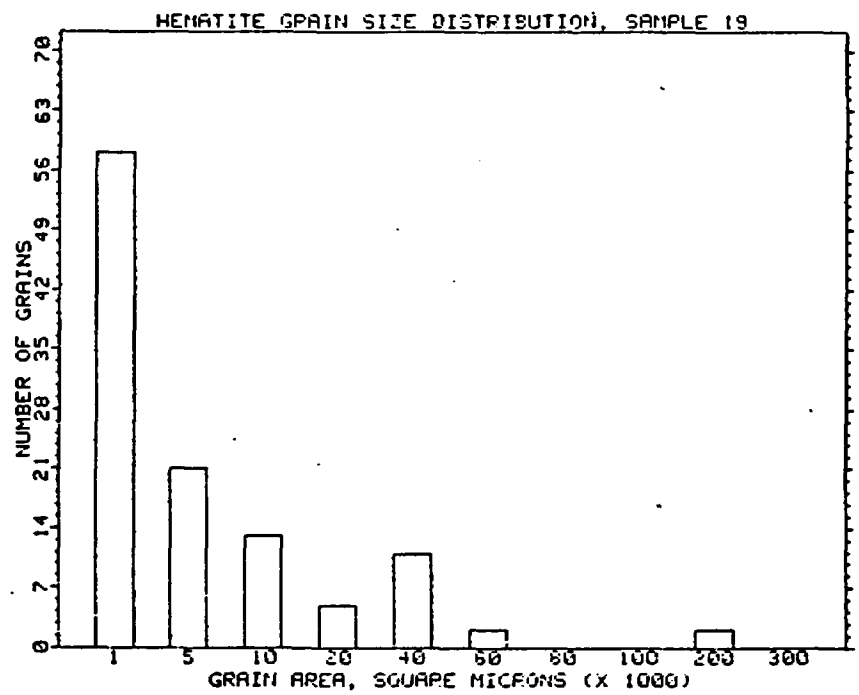

Figure A10.—Histogram of hematite grain-size distribution in sample 19 from drill hole UE25a-5, Nevada Test Site. Numbers below bars indicate maximum grain area in thousands of square microns.

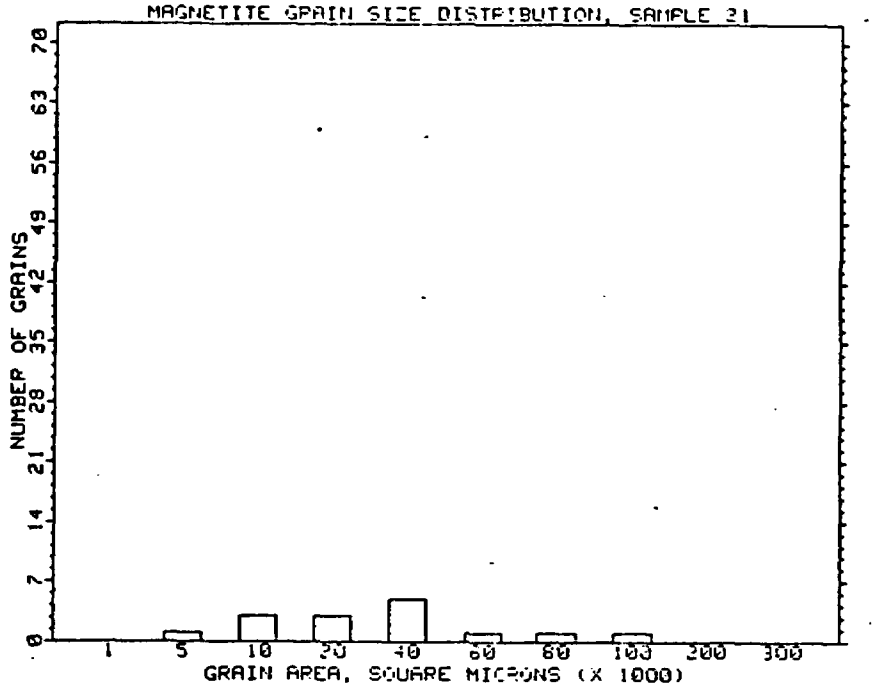

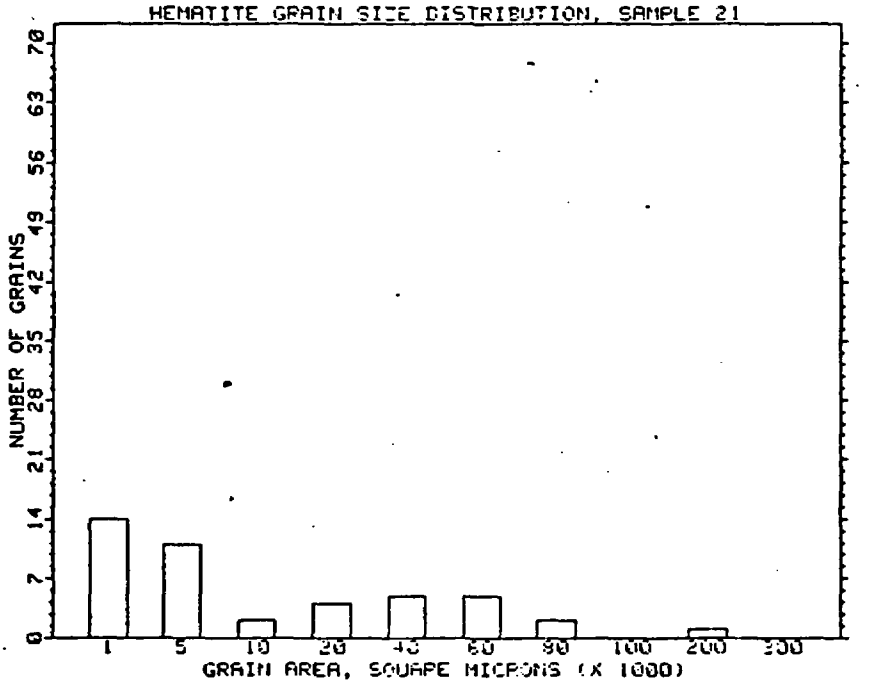

Figure A11.—Histogram of hematite and magnetite grain-size distributions in sample 21 from drill hole UE25a-5, Nevada Test Site. Numbers below bars indicate maximum grain area in thousands of square microns.

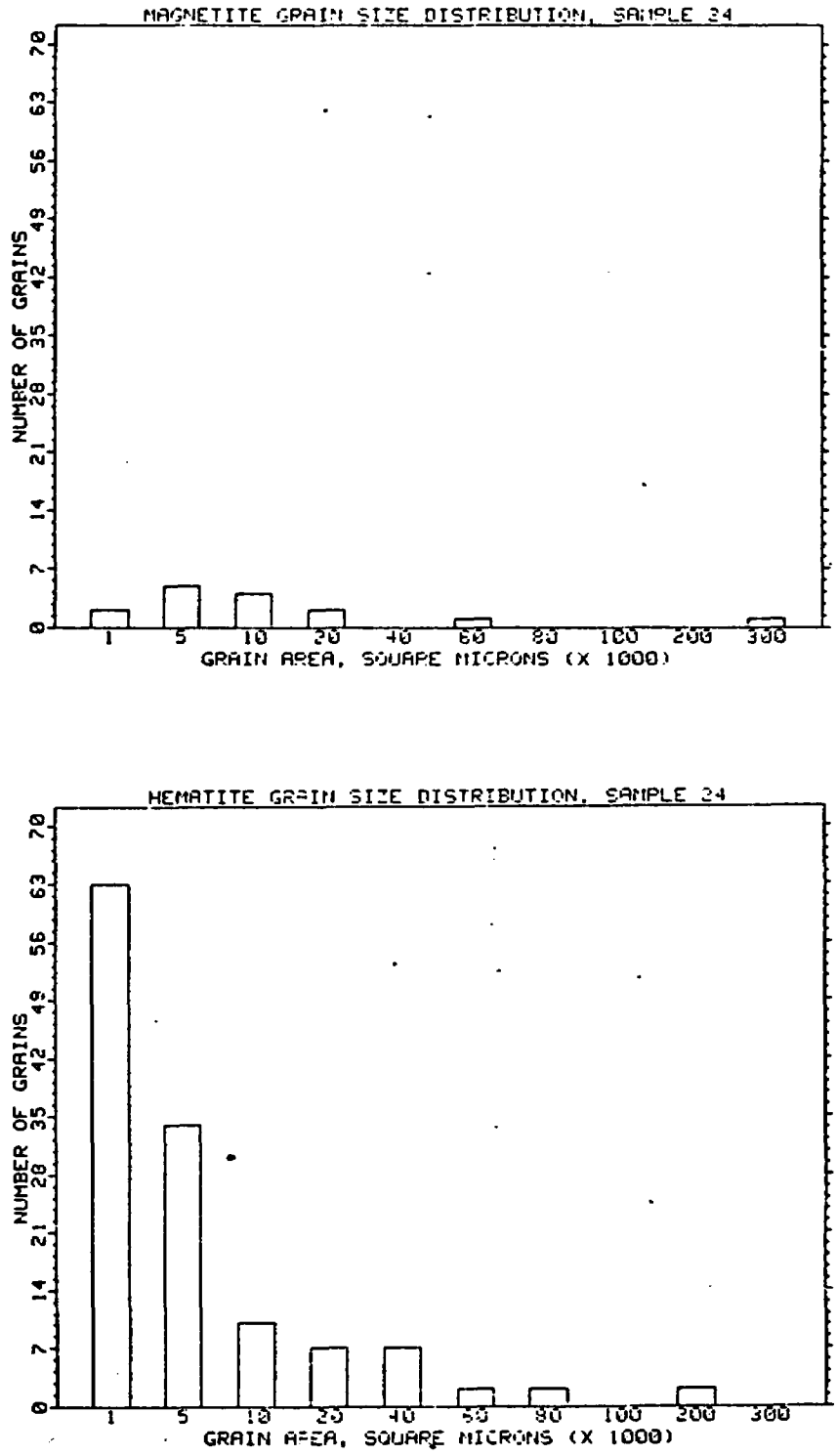

Figure A12.—Histogram of hematite and magnetite grain-size distributions in sample 24 from drill hole UE25a-5, Nevada Test Site. Numbers below bars indicate maximum grain area in thousands of square microns.

GPO 859-847